Nuclear Engineering and Technology 53 (2021) 3003–3011

Contents lists available at ScienceDirect

Nuclear Engineering and Technology

journal homepage: www.elsevier.com/locate/net

Original Article

Flow-accelerated corrosion assessment for SA106 and SA335 pipes with elbows and welds

Dong-Jin Kim*, Sung-Woo Kim, Jong Yeon Lee, Kyung Mo Kim, Se Beom Oh, Gyeong Geun Lee, Jongbeom Kim, Seong-Sik Hwang, Min Jae Choi, Yun Soo Lim, Sung Hwan Cho, Hong Pyo Kim

Materials Safety Technology Development Division, Korea Atomic Energy Research Institute (KAERI), 111, Daedeok-daero, 989 Beon-gil, Yuseong-gu, Daejeon, South Korea, 34057

ARTICLE INFO

Article history:
Received 4 September 2020
Received in revised form
22 March 2021
Accepted 24 March 2021
Available online 1 April 2021

Keywords:
Flow-accelerated corrosion
Pipe corrosion
Orifice
Elbow
Weld
Complicated fluid

ABSTRACT

A FAC (flow-accelerated corrosion) test was performed for a straight pipe composed of the SA335 Gr P22 and SA106 Gr B (SA106-SA335-SA106) types of steel with welds as a function of the flow rate in the range of 7–12 m/s at 150 °C and with DO < 5 ppb at pH levels ranging from 7 to 9.5 up to a cumulative test time of 7200 h using the FAC demonstration test facility. Afterward, the experimental pipe was examined destructively to investigate opposite effects as well as entrance effects. In addition, the FAC rate obtained using a pipe specimen with a 50 mm inner diameter was compared with the rate obtained from a rotating cylindrical electrode. The effects of the complicated fluid flows at the elbow and orifice of the pipeline were also evaluated using another test section designed to examine the independent effects of the orifice and the elbow depending on the distance and the combined effects on orifice and elbow. The tests were performed under the following conditions: 130–150 °C, DO < 5 ppb, pH 7 and a flow rate of 3 m/s. The FAC rate was determined using the thickness change obtained from commercial room-temperature ultrasonic testing (UT).

1. Introduction

Wall thinning in pipes made of SA106 due to flow-accelerated corrosion (FAC) is one of the major degradation phenomena in fossil and nuclear power plants. This has led to human injuries and economic losses due to accidents such as those at Surry Unit 2 in 1986 and Mihama Unit 3 in 2004 [1–3]. Research on pipe thinning has been active around the world with such accidents as a pivot point, and a number of experimental test facilities have been developed (e.g., EDF-CIROCO, France; AREVA-BENSON, Germany; B&W FAC Loop, Canada and CRIEPI-PRINTEMPS, Japan) to evaluate the various factors that affect pipe thinning [4–6].

FAC is usually affected by chemical parameters in aqueous environments, such as dissolved oxygen (DO), the flow velocity and the pH and temperature as well as by the pipe materials affected by those parameters [7,8]. Much of the research on FAC examines the effects of a single parameter on rotating coupon specimens [9,10]. However, the pipelines of a nuclear plant consist of numerous curved sections with elbows, valves and orifices by which the water flow is strongly disturbed, thereby leading to asymmetric fluid formation [11,12]. As a result, pipes can become asymmetrically thinned [13]. However, the effects of FAC on an asymmetric flow and related complex components have mainly been simulated using CFD (computational fluid dynamics) rather than by experiments [14–18].

Moreover, most studies have utilized small coupons or pipe pieces as samples for the experiments, which are not appropriate for non-destructive examinations (NDE) using ultrasonic testing (UT) despite the fact that plants use UT as a thickness measurement method [15,19–21].

In this study, pipes with an inner diameter of 50 mm (two inches) were subjected to UT as NDE. FAC tests were conducted on two types of test sections (a straight pipe test section composed of SA335 Gr P22 and SA106 Gr B: SA106-SA335-SA106) steels and a second test section to investigate the effects of the complicated fluid flows which form at the elbow and orifice of the pipeline. The FAC rate was determined using the thickness change obtained from commercial room-temperature ultrasonic testing (UT) before and

* Corresponding author.
E-mail address: djink@kaeri.re.kr (D.-J. Kim).

https://doi.org/10.1016/j.net.2021.03.026

after each test.

Higher FAC rate was observed in a low Cr steel at the weld area, compared with a low Cr steel far from the weld bead, irrespective of flow direction. This suggests that the weld bead area in the flowing direction from the carbon steel to the low alloy steel should be inspected carefully, comparable to the weld bead area in the flowing direction from the low alloy steel to the carbon steel (well known as the entrance effect) [22].

Moreover, a combined effect of the orifice and elbow on the FAC was demonstrated experimentally, showing the highest FAC rate and asymmetric FAC behavior compared to a straight pipe following a single orifice and a straight pipe flowing along a single elbow.

2. Experimental procedure

2.1. Test sections

A straight test section (pipe test section 1) with dissimilar metal welds between SA106 Gr B of 0.04 wt% Cr and SA335 Gr P22 of 2.08 wt% Cr (Table 1) composed of a 50 mm-inner-diameter pipe was designed as shown in Fig. 1 to investigate the entrance effect (SA335-SA106) and the opposite effect (SA106-SA335). The distance from the dissimilar welds was designed to be 15 times greater than the inner diameter of the two-inch pipe.

To measure the thinning phenomenon in various parts of the pipeline, a second test section (pipe test section 2) was designed to have an elbow (radius of 76 mm, SA234WPB equivalent to SA106) and a 40-mm-diameter orifice, as presented in Fig. 2. Each section is defined as follows: W–P03, the straight pipe section following orifice 1, W-E01, the first elbow section, W–P04, the straight pipe section following the first elbow (W-E01) and W-E02, and the second elbow section following orifice 2.

W–P03, W-E01 and W–P04 were designed to evaluate the effect of the distance from the orifice and from the elbow on pipe thinning, respectively. W-E02 was designed to allow the observation of the pipe-thinning phenomena associated with the complicated flow caused by the combined conditions of the orifice and the elbow (Fig. 2).

GTAW (gas tungsten arc welding) was carried out using EWTh-2 and ER70S-6 as a tungsten electrode and a filler metal, respectively, for the straight pipe weld and the straight pipe/elbow weld at an interpass temperature in the range of 170–190 °C at an Ar gas flow rate of 10–15 L/min. In total, three layers were welded in the input current and voltage ranges of 90–100 A and 11–12 V for the first layer and 140–170 A and 12–14 V for the other layers, respectively. A post-heat treatment was not carried out. Soundness of the weld was confirmed by PT (liquid penetration testing) and RT (radiographic testing) examinations. After welding the metal with 0.15 wt % Cr (ER70S-6), the back bead inside the pipe was machined and then selectively removed while avoiding damage to the base material.

Regarding the plate coupon test, a rotating cylindrical electrode with a 120 mm diameter was designed to rotate in an autoclave connected to motor outside. Plate-type specimens were attached to a rotating cylinder with a gap of 3.5 mm between the rotating cylinder and the autoclave wall, following an earlier procedure [10,23].

Table 1
Chemical composition of the pipe materials (wt%) as manufactured by Nippon Steel & Sumitomo Metal Corporation.

Alloy	C	Si	Mn	Cu	Cr	Ni	Mo	Fe
SA106 Gr B	0.19	0.24	0.98	0.02	0.04	0.02	0.01	Bal.
SA335 Gr P22	0.1	0.22	0.42		2.08		0.94	Bal.

2.2. FAC test and thickness measurement

The straight pipe test section (pipe test section 1) was exposed to the conditions of 150 °C, DO < 5 ppb in a pH range from 7 to 9.5 as a function of the flow rate in the range 7–12 m/s with 1200 h for each run using the FAC demonstration test facility designed and manufactured by the Korea Atomic Energy Research Institute (KAERI) in 2016 [24]. In total, six runs were performed up to a cumulative test time of 7200 h for pipe test section 1. After the experiment, the pipe was examined destructively to investigate the entrance and opposite effects.

A test was also performed during 1100–1200 h under the conditions of 130–150 °C, DO < 5 ppb, pH 7 and a flow rate of 3 m/s for the second test section with an orifice and elbow (pipe test section 2).

The flow rate was determined from the volumetric flow divided by the flow area for the pipe. A 10 m/s flow rate corresponds to 1141 L/min in the experimental system.

Deaeration was achieved by nitrogen purging in a water tank, after which deaerated water was pumped into the test section using an injection pump. Let-down water of the same amount was then flowed into an ion exchanger for purification and then back to the water tank. The system pressure is controlled by a pressurizer. A high-pH experiment is carried out through an additional ammonia injection into the chemical tank before the injection pump operates.

The pipe thickness was measured ten times using a commercial room-temperature UT (Olympus 38DL Plus, resolution 10 μm) in the center of each grid (15 × 15 mm) before the experiment. The grid was drawn along the length and circumference of the straight pipe and elbow prior to the experiment. Every UT measurement was carried out after calibration using a SS304 block.

For the rotating cylindrical electrode experiment, the FAC test was performed at 150 °C and with inlet water at a pH of 7 as a function of the flow rate up to 3000 h. The test solution is circulated to control the pH and to remove dissolved ionic species with a flow rate of 50 cc/min through a test loop equipped with an ion exchanger. Dissolved oxygen below 5 ppb was controlled by nitrogen purging throughout the experiment. The FAC rate was determined from the weight loss after the test [10,23]. It should be noted that the flow rate was determined from the peripheral velocity for a rotating cylinder electrode, unlike the flow rate for the pipe specimen mentioned above.

The straight pipe test section was destructively examined to observe its surface morphology and surface oxide by means of optical microscopy (OM) and TEM (transmission electron microscope, JEM-2100F, JEOL) for specimens prepared using a FIB (focused ion beam). Entrance and opposite effects at the weld areas were also investigated using CT (computed tomography). The characteristics of the surface and the cross-section of the plate coupon specimen from the rotating cylindrical electrode were observed using OM and TEM for samples prepared with a method identical to that used for the straight pipe specimen and the results were compared.

3. Results and discussion

Fig. 3 shows the wall thinning outcome of SA106 as measured from the middle region of the pipe with the flow direction as a function of the flow velocity during 1200 h in each test. The thinning rate increased with the flow velocity irrespective of the SA106-SA335 (P22) or SA335 (P22)-SA106 flow direction. The FAC rates

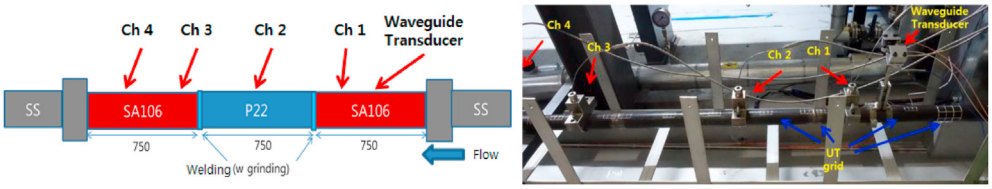

Fig. 1. Schematic and photograph of the experimental straight pipe test section.

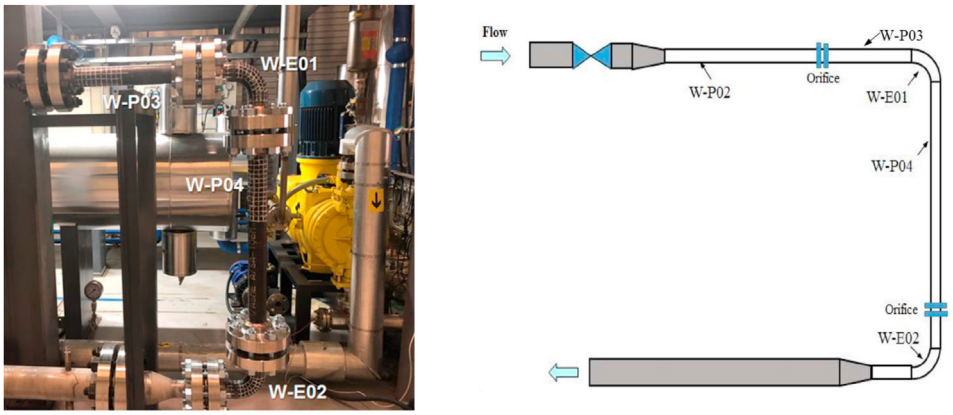

Fig. 2. Photograph and schematic of the test section with the orifice and elbow.

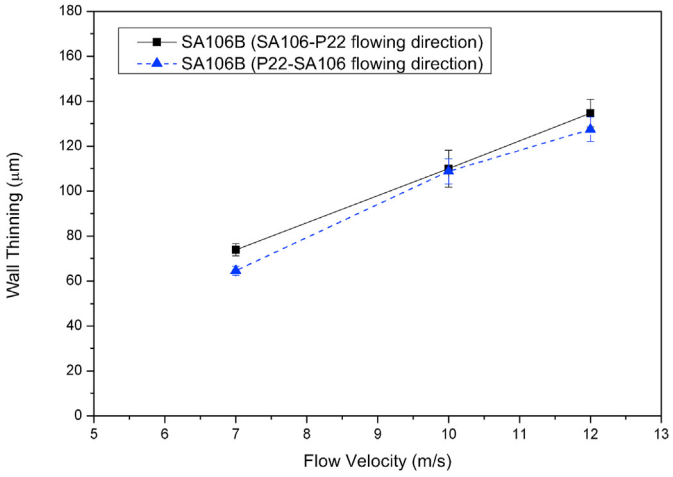

Fig. 3. Wall thinning of SA106 measured from the middle region of the pipe with the flow direction as a function of the flow velocity during 1200 hrs in each test.

obtained from the straight pipe test section and rotating cylindrical electrode are shown in Table 2 [10,24]. It has been reported [25–27] that the FAC rate remains constant over time, except for the initial period of tens of hours. In this work, every experiment using a pipe test section and the coupon tests using the rotating electrode lasted 1200 and 3000 h, respectively, durations which are long enough to attain a steady state. Therefore, the total wall thickness change for the test was converted to the average FAC rate (mm/yr) in this work.

Table 2
Average FAC rate and Reynolds number for the rotating cylindrical electrode and straight pipe test section with the flow rate.

Flow rate (m/s)	2	4	7	10	12
FAC rate (mm/yr) for cylindrical specimen	**0.83**	**1.38**		**9.1**	
Reynolds number (xE6) for cylindrical specimen	**1.1**	**2.2**		**5.5**	
FAC rate (mm/yr) for pipe specimen			**0.54**	**0.8**	**0.99**
Reynolds number (xE6) for pipe specimen			**1.6**	**2.3**	**2.7**

The FAC rate increased with the flow rate for the carbon steel (SA106 Gr B) irrespective of the testing method used (i.e., rotating cylindrical electrode or pipe test section). There was a significant difference between the FAC rates with the experimental method at an identical flow rate, e.g., 9.1 mm/yr and 0.8 mm/yr for the cylindrical coupon test and pipe specimen at a flow rate of 10 m/s, respectively. However, it was also found that the range of the FAC rates with the experimental method became much narrower when the Reynolds numbers as determined in the experimental condition were similar to each other (The FAC rate (1.38 mm/yr in the coupon test) for a Reynolds number of 2.2×10^6 is similar to the FAC rate (0.8 mm/yr for the pipe specimen) for a Reynolds number of 2.3×10^6) considering the broad data scattering of the FAC rate.

It was also noted that the Reynolds number is defined as the density x mean velocity x hydraulic diameter/dynamic viscosity. The density, mean velocity, hydraulic diameter and dynamic viscosity are the water density at the test temperature (150 °C in this work), the average flow velocity, the diameter of the flow and the dynamic viscosity of the water at the test temperature (150 °C in this work), respectively. The mean velocity is determined from the volumetric flow divided by the flow area for the pipe and from the peripheral velocity of the rotating cylinder. The diameter refers to the cylinder diameter (120 mm) of the rotating cylinder as well as the inner diameter (50 mm) of the pipe.

It is presumed that the geometry differs greatly between the two experimental methods, leading to different hydrodynamic conditions. Accordingly, it appears that the FAC rate is more closely related to the hydrodynamic parameter than to the apparent flow rate. Chen et al. reported [25] that the corrosion rate for a flow-through pipe channel, annular flow channel and a rotating cylinder system was independent of the geometry when plotted as a function of the mass transfer coefficient on a log-log scale. This indicates that hydrodynamic parameters containing geometrical

information such as the mass transfer coefficient and Reynolds number are more important with regard to the FAC rate than the apparent flow rate and should be considered in a FAC analysis.

Fig. 4 shows an OM image taken after the experiment with the straight pipe test section (pipe test section 1). A typical orange-peel surface texture was observed on the SA106 specimen but not observed with P22 (SA335), whereas the orange peel texture was not found on the rotating cylindrical electrode irrespective of the Cr content in the alloy during the test up to 3000 h [23]. It appears that the surface texture difference stems from the experimental method despite the fact that the Reynolds numbers are similar and the flow is in the same regime (turbulence regime). The precise turbulence pattern of the rotating electrode is not identical to that of the pipe. This difference from the experimental method should be clarified in the future.

The cross-sectional morphologies obtained from the TEM sample prepared using the FIB are correspondingly presented in Figs. 5 and 6 for the pipe and rotating electrode specimens. Both of the surface oxides which formed during the test are not dense compared to the dense image of the metal side. The oxide thicknesses do not differ greatly in the range of 1–2 μm irrespective of the experimental method used, unlike the difference in the surface texture for these two dissimilar specimens (i.e., the straight pipe and rotating coupon. Hence, the oxide formation behavior depends less on the turbulence pattern, unlike the surface texture.

Fig. 7 presents a CT image of the straight pipe section, specifically showing the SA106-SA335 (P22) flow direction. A weld bead on the outside was noted, whereas an inside weld bead is absent because the weld bead inside the pipe after welding was removed before the experiment to investigate the effect of the chemical composition on the FAC, as mentioned in the experimental section. There was a thickness difference of 470 μm between the P22 and SA106 cases due to the different FAC rates caused by the Cr content difference (2.08 wt% for SA335 and 0.04 wt% for SA106) during the experiment. There is only a slight thickness change for P22 with a relatively high Cr content. According to the room-temperature UT

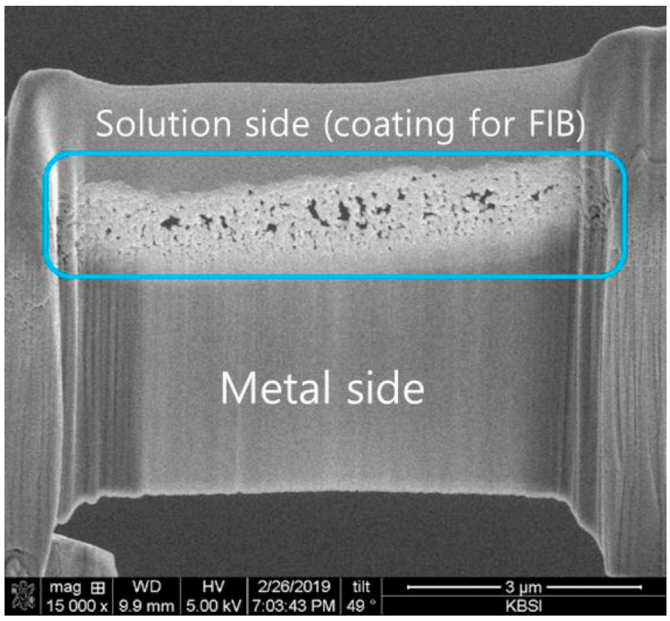

Fig. 5. TEM image from the SA106 specimen prepared using a FIB from the straight pipe test section after a cumulative experimental duration of 7200 hrs.

and the results shown in Fig. 3, the cumulative thinned thickness during the entire experiment of 7200 h was approximately 420 μm, similar to the value of 470 μm from the destructive examination.

It is interesting that there was a steep barrier wall at the boundary between the weld metal and the SA106 material. The weld metal of 0.15 wt% Cr is resistant to FAC in water at pH 7 and 150 °C, while SA106 with 0.04 wt% Cr is relatively readily thinned during the experiment. Consequently, a barrier layer approximating a wall would be produced due to the difference in the corrosion rate in the initial stage, after which the wall serves to

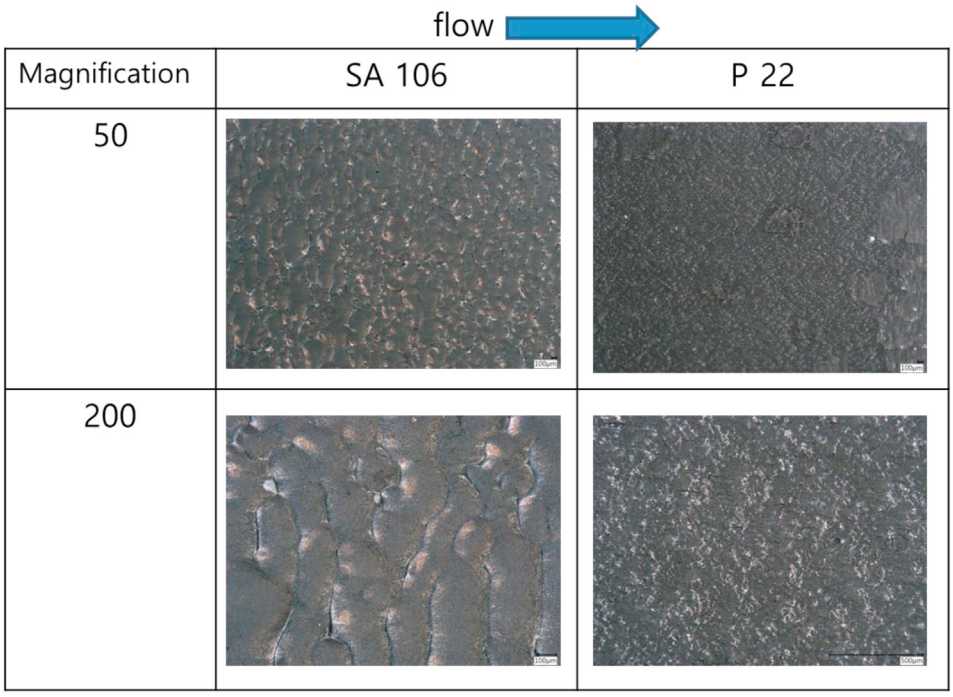

Fig. 4. Optical microscopy images after a cumulative experimental duration of 7200 hrs with the straight pipe test section.

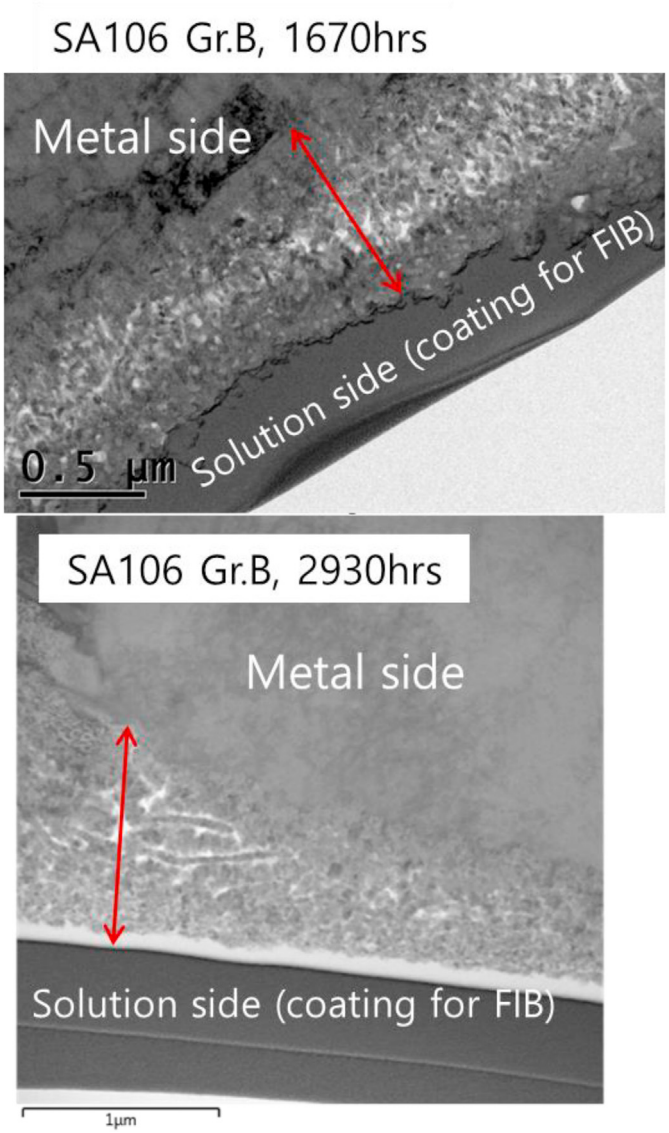

Fig. 6. TEM image of the SA106 specimen prepared using a FIB for a rotating cylindrical electrode.

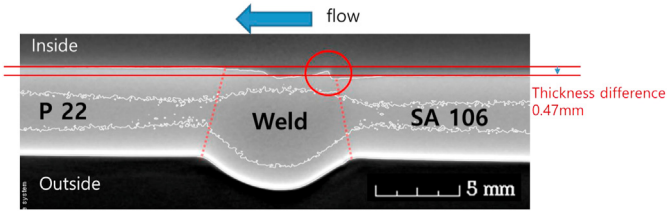

Fig. 7. CT image of the section with the flow in the SA106-P22 direction obtained after a cumulative experimental duration of 7200 hrs.

create additional turbulence, such as an eddy flow, causing FAC acceleration near the boundary wall. It should also be noted that the FAC rate was more increased for SA106 closer to the boundary wall due to additional turbulence.

Accordingly, it is suggested that the FAC acceleration effect should be carefully considered for dissimilar welds when cooling water flows in the low Cr alloy to the high Cr alloy direction. Barrier layer formation and hence the FAC acceleration effect may also be facilitated by galvanic corrosion caused by electrochemical potential difference between the low Cr alloy and high Cr alloy. This wall thinning behavior caused by the local thinning rate difference was not discriminated in the UT data which can be obtained from the wider area relative to the local hump area.

On the other hand, higher FAC was also observed at weld bead area for the opposite flow direction (SA335 (P22)-SA106), as shown in Fig. 8. It is known that the entrance effect occurs when single-phase water flows from a resistant material to a susceptible material [22]. The susceptible low Cr material dissolves easier than a resistant material with a high Cr level in water. Water flowing along a resistant material contains fewer Fe ions than water from a susceptible material. The Fe ion concentration gradient at the boundary region between a resistant material with a high Cr level and a susceptible material with a low Cr level is caused by the different dissolution rates between the two materials, providing the driving force for the additional dissolution of the susceptible material. Therefore, a susceptible material at the boundary between a resistant material and a susceptible material thins more rapidly.

The weld metal, more susceptible than P22 (SA335), and SA106, more susceptible than the weld metal, were thinned more at the boundary, indicating an entrance effect. However, it is worthwhile to note that there is slight difference in shape of the weld bead area with the flow direction, compared with Fig. 7. An obvious steep barrier wall was not observed in Fig. 8 unlike inset circle in Fig. 7. It is reasonable that a steep barrier wall does not form easily when water flows from the high Cr steel (low FAC rate) to the low Cr steel (high FAC rate) (water flow in the downhill direction).

Apart from water flow in the downhill direction, when water flows from the susceptible low Cr steel to the resistant high Cr steel (water flow in the uphill direction), initially the difference in FAC from high to low rate caused by the chemical compositional difference may introduce a shallow barrier layer such as a wall, after which a steeper wall such as a high hump develops relatively easily due to the additional turbulence caused by the wall, leading to locally rapid thinning over time.

Considering long-term maintenance aspects, the opposite effect (susceptible material to resistant material direction of flow) would be also a significant threat with regard to pipe thinning, comparable to the well-known entrance effect (resistant material to susceptible material direction of flow) which is regarded as an important wall thinning phenomena. Nevertheless, more precise experimental data to support this result are needed for generalization of the opposite effect. Moreover it seems that the difference in width of the two welds in Figs. 7 and 8 can also somewhat contribute to the profile development of weld bead area.

At this point, we discuss the experimental result using pipe test section 2. Fig. 9 shows the FAC rate with the distance of a straight pipe following the first orifice (W–P03) for the second test section including an orifice and an elbow. The error bar indicates the

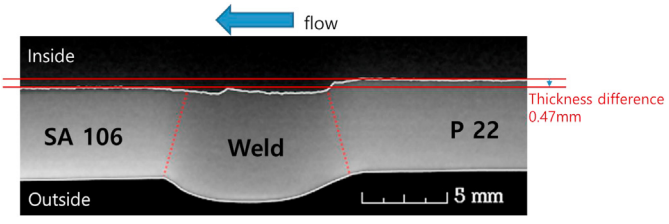

Fig. 8. CT image of the section with the flow in the P22 (SA335)-SA106 direction obtained after a cumulative experimental duration of 7200 hrs.

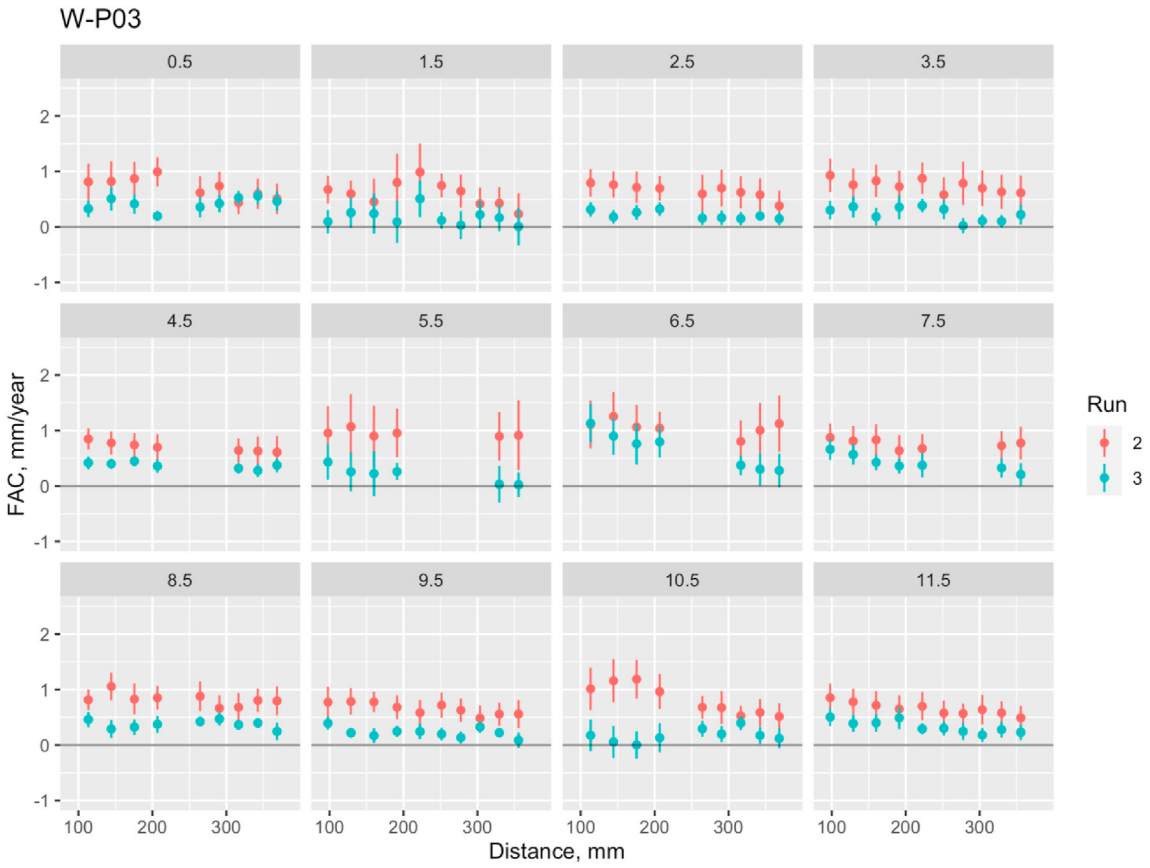

Fig. 9. FAC rate with the distance of a straight pipe following the first orifice (W–P03) for the second test section.

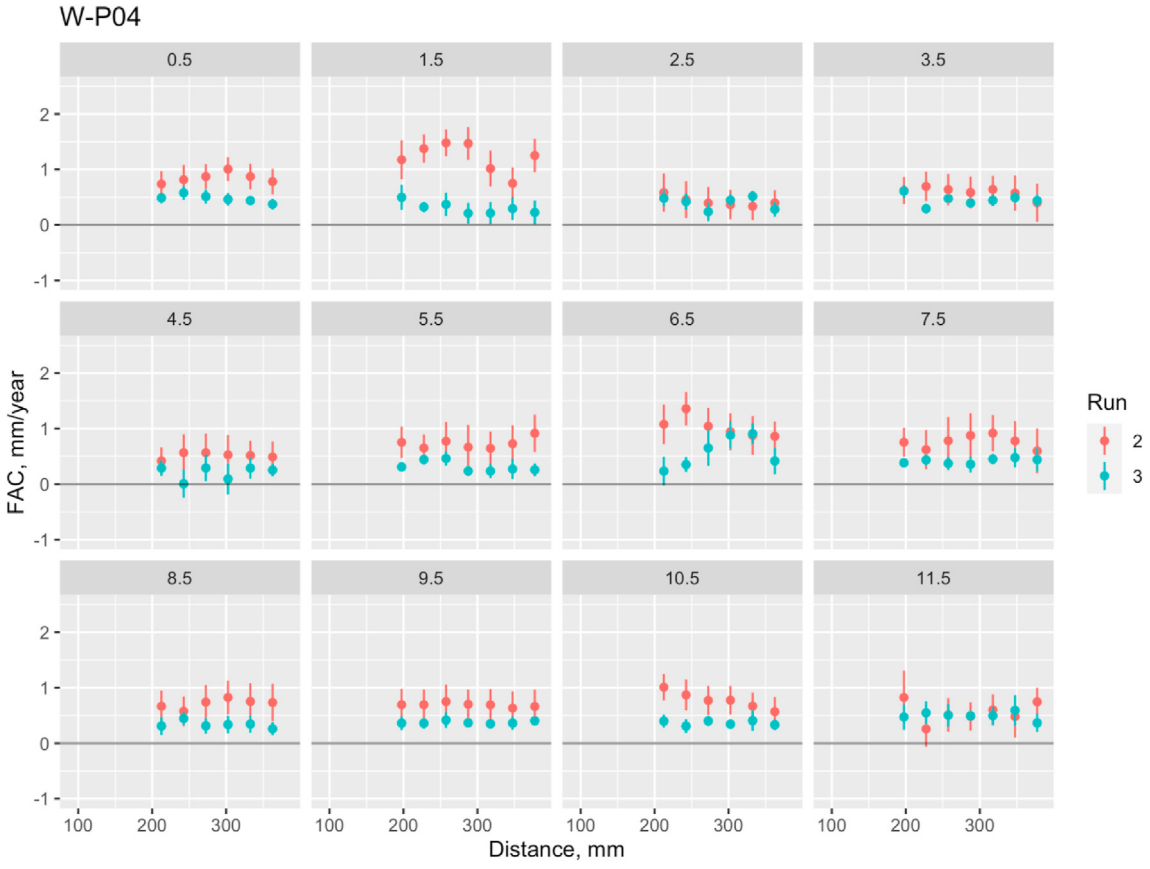

Fig. 10. FAC rate with the distance of the straight pipe following the first elbow (W–P04) for the second test section.

standard deviation of the UT data in Figs. 9–12. Runs 2 and 3 represent the experimental tests performed at 150 °C and 3 m/s for 1100 h and at 130 °C and 3 m/s for 1200 h, respectively.

It is convenient to explain the circumferential position of the pipe over time when water flows along the pipe. The top and bottom edges as the angular positions refer to 0 and 6 o'clock, respectively. Right and left edges as the angular positions similarly denote 3 and 9 o'clock. Therefore, each time and distance in the W–P03 case will indicate a UT grid point along the circumference of pipe and the distance from the orifice, respectively.

The FAC rate of Run 2 is higher than that of Run 3. FAC dependency on the temperature is known to balance the reaction rate related Fe ion solubility and the mass transfer related to the diffusion of ionic species. Earlier work reported [9] that the FAC rate is highest near 150 °C, consistent with this work. The FAC rate decreased slightly with the distance and then remained constant after 300 mm (around 6D, where D is the inner diameter of the pipe). Another report found [20] that the FAC rate decreased to a constant level after 4D according to measurements of the plate thickness using an electrochemical method.

There appears to be a higher FAC rate at 1.5, 5.5 and 10.5 at the angular positions in the radial direction, indicating that positions near the top and bottom are readily thinned compared to other circumferential positions after the first orifice. This can be related to the geometry of the test section or the symmetric position of the orifice assembled before the test. The FAC rate based on UT data will be analyzed through a CFD program and via a destructive examination in the future.

Fig. 10 shows the FAC rate with the distance for the straight pipe following the first elbow (W–P04) of the second test section. Each time and distance value in the W–P04 case indicates a UT grid point along the circumference of the pipe and the distance from the elbow, respectively. The FAC rate of Run 2 is also higher than that of Run 3, as with the W–P03 section. The FAC rate decreased slightly with the distance, but was as high as to 380 mm (around 7.6D, where D is the inner diameter of the pipe), greater than that in the W–P03 section. This indicates that the change in the flow distribution caused by an elbow leads to a longer distance in the straight pipe section compared to the flow distance modified by an orifice. Higher FAC rates at 1.5 and 6.5 as angular positions are likely, an outcome somewhat consistent with the W–P03 results. The data distribution at 1.5 for Run 2 was wider than that in the W–P03 section. This may be due to the development of an asymmetric flow caused by the elbow.

Figs. 11 and 12 show the FAC rate with the angle from the entrance to the exit of the first elbow (W-E01) for the second test section and the FAC rate with the angle of the second elbow (W-E02) following the second orifice in the second test section, respectively. For the elbow, it is convenient to explain the distance from the entrance to the exit of the elbow as the angles of the elbow of 0° and 90°, respectively. It is also convenient to explain the circumferential position of the elbow over time when water flows along the elbow. The top and bottom edges refer to 0 and 6 o'clock as the angular positions, respectively. Similarly, the right and left edges refer to 3 and 9 o'clock as the angular positions.

The FAC rate of Run 2 is also higher than that of Run 3, as with the straight pipes and the W–P03 and W–P04 sections at the first elbow (W-E01). It was also noted that the FAC rate is higher and widely distributed at 0 and 0.9 as the angular positions, compared to the outcomes at other positions. The FAC rate decreased with the

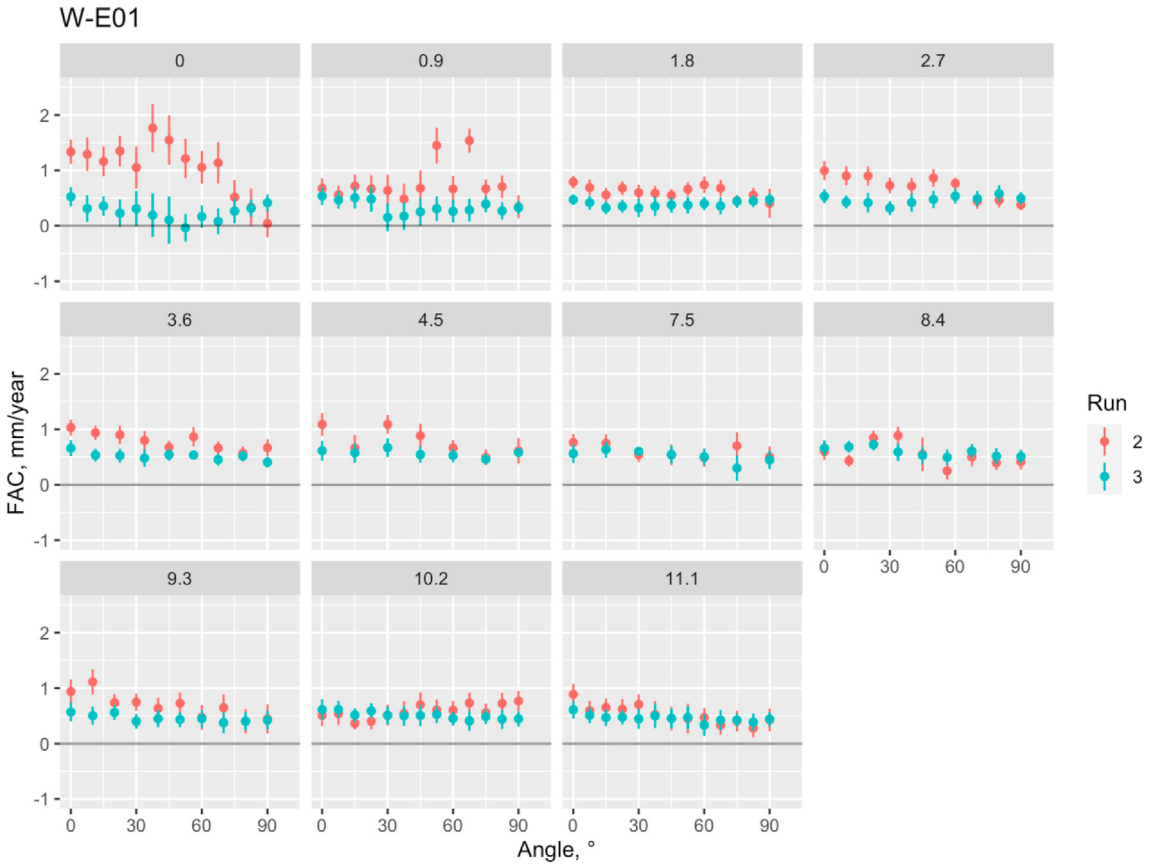

Fig. 11. FAC rate with the radial angle of the first elbow (W-E01) for the second test section.

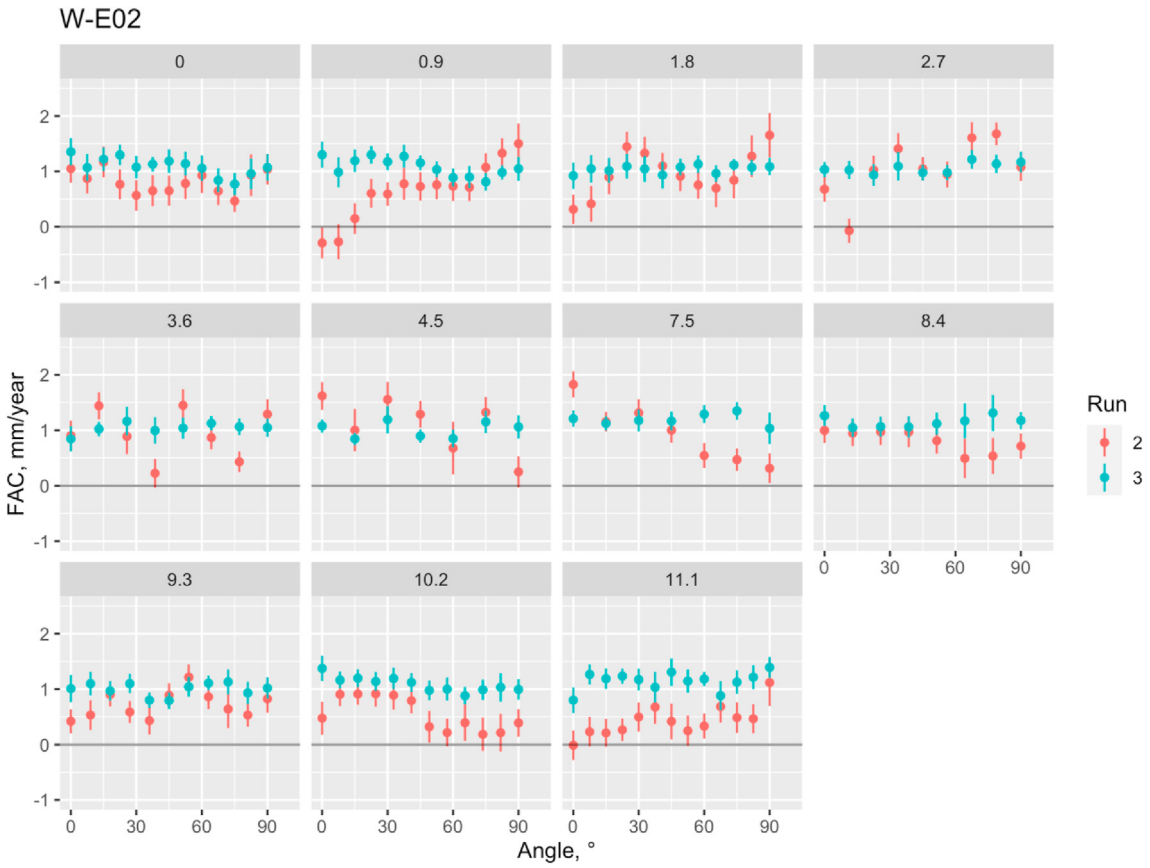

Fig. 12. FAC rate with the radial angle of the second elbow (W-E02) following the second orifice for the second test section.

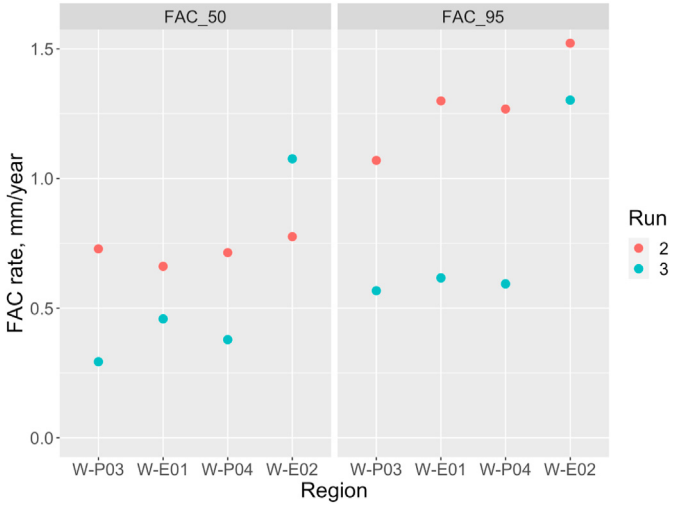

Fig. 13. FAC rate for various sections at 50 and 95 percentiles in the data.

angle (distance). It has been reported [14,16,18] that the angular velocity is highest at the intrados of the elbow, with CFD simulations used to assess this via a combination of the turbulent intensity, velocity and shear stress terms.

From the result in Fig. 11, based on room-temperature UT data, it appears that the extrados is more susceptible to FAC than the intrados. It also appears that the wide distribution is due to the complicated flow caused by the elbow. The high FAC rate near the extrados is related to the high FAC rate near the top area (1.5 as the angular position in Fig. 10) for W–P04 following W-E01. However, FAC is not high near 6.5 as the angular position for W-E01, where the FAC rate was found to be higher than at other positions for W–P04 (6.5 as the angular position in Fig. 10), meaning that other flows would be generated toward the bottom area of W–P04 when water flows into the straight pipe along the elbow.

In Fig. 12, obtained from the second elbow (W-E02), the FAC rate varies most widely among the four sections (W–P03, W–P04, W-E01 and W-E02), indicating the combined effect of the orifice and elbow. The FAC rate changed with the angle of the elbow; it increased at 0.9 and 11.1 as the angular positions near the extrados but decreased relatively at 7.5 and 10.2 as the angular positions for Run 2 when cooling water flowed from the entrance to the exit. The nonuniformity of FAC rate for W-E02 increased with the angle (distance) compared to that for W-E01. Given this different behavior between the W-E01 and W-E02 sections, it is likely that the flow became more asymmetric under the combined effect of the orifice and elbow compared to the effect of a single elbow.

The circumferential position at which the FAC occurs rapidly varies with the components, such as the orifice, elbow, straight pipe and combinations of these components. This will be elaborated on via destructive examinations of straight pipes and elbows in the future.

Fig. 13 shows the FAC rate as a function of section (W–P03, W–P04, W-E01 or W-E02) for Run 2 and Run 3 as the 50th and 95th percentiles of the data. It was found that Run 2 at 150 °C and 3 m/s resulted in a wider data band compared to Run 3 at 130 °C and 3 m/s according to a comparison of the 50th and 95th data percentiles. The width of the data band is consistent with the FAC rate, which was higher for Run 2 than Run 3. The data band was widest in the

W-E02 section in particular, which is related to the complexity of the flow.

The FAC rate increased in the order of W–P03 < W–P04 < W-E01 < W-E02 from the 95th percentile data. It should also be noted that the highest FAC rate was obtained at the elbow following the orifice, indicating a synergistic effect of the complex flow developed from the combination of the orifice and elbow compared to those at a single elbow or a single orifice on the FAC. The FAC rate based on UT data in this work requires additional analyses through CFD programs and destructive examinations.

4. Summary

1) A typical orange-peel surface texture was observed for a straight pipe SA106 specimen, whereas the orange peel texture was not found for the rotating cylindrical electrode in earlier work. Unlike the difference in the surface appearance, an oxide morphology showed similar patterns in terms of the thickness and porosity irrespective of the experimental method used with the pipe specimen and rotating electrode.
2) Higher FAC rate in a low Cr steel at the weld bead area was found, compared with a low Cr steel far from the weld bead, irrespective of flow direction (from high to low Cr alloy (entrance effect) and from low to high Cr alloy (opposite effect)) for a straight pipe test section.
3) The FAC rate increased in the order of 'straight pipe following a single orifice', 'straight pipe following a single elbow', 'single elbow' and 'elbow following the orifice' (W–P03 < W–P04 < W-E01 < W-E02) from the 95th percentile data, indicating a synergistic effect on the FAC of the flow caused by the combined conditions of the orifice and elbow, as opposed to a single elbow or a single orifice.

Declaration of competing interest

All authors have no conflicts of interest to declare.

Acknowledgements

This work was financially supported by the Korean Nuclear R&D Program organized by the National Research Foundation (NRF) with support from the Ministry of Science and ICT (2017M2A8A4015155) and by the R&D Program of the Korea Atomic Energy Research Institute (KAERI).

References

[1] H. Keller, Erosionskorrosion an nassdampfturbinen, VGB-Kraftwerkste 54 (1974) 292–295.
[2] R.B. Dooley, V.K. Chexal, Int. J. Pres. Ves. Pip. 77 (2000) 85–90.
[3] T. Sydberger, U. Lotz, J. Electrochem. Soc. 129 (1982) 276–283.
[4] H. Schmidt, W. Kohler, W. Kastner, High-Pressure Test Facility-25 Years of Operation, Framatome ANP GmbH Report (2001). March.
[5] E.M. Pavageau, R. Michel, Influence of Chemistry and Temperature on the FAC Rate of Carbon Steel, in: presented at Int. Conf. on FAC, March 18-20, Lyon, France, 2008.
[6] Y.S. Lee, S.H. Lee, K.M. Hwang, Corrosion Science and Technology 15 (2016) 182–188.
[7] E.H. Lee, K.M. Kim, H.P. Kim, Corrosion Science, and Technology 12 (2013) 280–287.
[8] L. Dejoux, M. Personz, S. Trevin, T. Knook, Flow Accelerated Corrosion Wall Thinning Management at EDF, in: presented at Int. Conf. on FAC, May 4-7, Lion, France, 2010.
[9] Flow Accelerated Corrosion in Power Plants, *EPRI Report*, TR-106611-R1, Palo Alto, CA, 1998.
[10] D.-J. Kim, K.M. Kim, J.H. Shin, Y.M. Cheong, E.H. Lee, G.G. Lee, S.W. Kim, H.P. Kim, M.J. Choi, Y.S. Lim, S.S. Hwang, Arch. Metall. Mater. 62 (2B) (2017) 1383–1387.
[11] D.H. Lister, L. Liu, A. Feich, M. Khatibi, W. Cook, K. Fujiwara, E. Kadoi, T. Ohira, H. Takiguchi, S. Uchida, Effects of Dissolved Oxygen on Flow Accelerated Corrosion in Feedwater Systems, in: Proceedings of the 13th International Conference on Environmental Degradation of Materials in Nuclear Power Systems-Water Reactors, Whistler, BC, Canada, August 2007.
[12] M. Ohkubo, T. Yamagata, S. Kanno, N. Fujisawa, Trans. JSME Ser. B77 (2011) 386–394.
[13] K. M Hwang, T.E. Jin, K. H Kim, J. Nucl. Sci. Technol. 46 (2009) 469–478.
[14] H.P. Rani, T. Divya, R.R. Sahaya, V. Kain, D.K. Barua, Ann. Nucl. Energy 69 (2014) 344–351.
[15] L. Zeng, G.A. Zhang, X.P. Guo, C.W. Chai, Corrosion Sci. 90 (2015) 202–215.
[16] S. Ebara, H. Takamura, H. Hashizume, H. Yamano, Int. J. Hydrogen Energy 41 (2016) 7139–7145.
[17] L. Xu, Q. Zhang, J. Zheng, Y. Zhao, Powder Technol. 302 (2016) 236–246.
[18] J. Tian, H. Huang, Z. Pan, H. Zhou, Trans. Nonferrous Metals Soc. China 26 (2016) 2857–2867.
[19] B. Clark, A. Feicht, A. Justason, D. Lister, The Effectiveness of Titanium Additions in Mitigating FAC under PWR Feedwater Conditions, in: presented at Int. Conf. on FAC, May 4-7, Lyon, France, 2010.
[20] Y. Nagaya, A. Nakamura, Y. Utanohara, M. Nurase, Evaluation of the Flow Accelerated Corrosion Downstream of an Orifice, in: presented at Int. Conf. on FAC , May 4-7, Lyon, France, 2010.
[21] K. Yoneda, K. Fujiwara, R. Morita, M. Satake, Y. Uchiyama, S. Watanabe, F. Inada, Research Activities on FAC Prediction in CRIEPI, in: presented at Int. Conf. on FAC, May 24-27, Lille, France, 2016.
[22] H. Crockett, J. Horowitz, Entrance Effect, in: presented at Int. Conf. on FAC, March 18-20, Lyon, France, 2008.
[23] D.J. Kim, M.J. Kim, K.M. Kim, S.W. Kim, H.P. Kim, S.S. Hwang, Evaluation of FAC for Rotating Cylindrical Carbon Steel, in: presented at Int. Conf. on FAC, May 24-27, Lille, France, 2016.
[24] K.M. Kim, Y.M. Choeng, E.H. Lee, J.Y. Yeon, S.B. Oh, D.J. Kim, Corrosion Science and Technology 15 (2016) 245–252.
[25] T.Y. Chen, A.A. Moccari, D.D. Macdonald, Corrosion 48 (1992) 239–255.
[26] E. H. Lee, K. M. Kim, H. P. Kim and D. J. Kim, Corrosion Science and Technology, 14 (2105) 25-32.
[27] Y.M. Cheong, K.M. Kim, D.J. Kim, Nuclear Engineering and Technology 49 (2017) 1463–1471.